

Evidence for surface defect passivation as the origin of the remarkable photostability of unencapsulated perovskite solar cells employing aminovaleric acid as a processing additive

Chieh-Ting Lin^{ab}, Francesca De Rossi^c, Jinhyun Kim^a, Jenny Baker^c, Jonathan Ngiam^b, Bob Xu^b, Sebastian Pont^a, Nicholas Aristidou^a, Saif A. Haque^a, Trystan Watson^c, Martyn A McLachlan^{*b}, James R Durrant^{*ac}.

a. Department of Chemistry and Centre for Plastic Electronics, Imperial College London, Exhibition Road, London SW7 2AZ, U.K

b. Department of Materials and Centre for Plastic Electronics, Imperial College London, Exhibition Road, London SW7 2AZ, U.K.

c. SPECIFIC IKC, College of Engineering, Swansea University, Bay Campus, Fabian Way, Swansea SA1 8EN, U.K.

Corresponding author:

Martyn A McLachlan (martyn.mclachlan@imperial.ac.uk)

James R Durrant (j.durrant@imperial.ac.uk)

1 **Abstract**

2 This study addresses the cause of enhanced stability of methyl ammonium lead iodide when
3 processed with aminovaleric acid additives (AVA-MAPbI₃) in screen printed, hole transport
4 layer free perovskite solar cells with carbon top electrodes (c-PSC). Employing AVA as an
5 additive in the active layer caused a 40-fold increase in device lifetime measured under full
6 sun illumination in ambient air (RH ~15%). This stability improvement with AVA was also
7 observed in optical photobleaching studies of planar films on glass, indicating this
8 improvement is intrinsic to the perovskite film. Employing low-energy ion scattering
9 spectroscopy, photoluminescence studies as a function of AVA and oxygen exposure, and a
10 molecular probe for superoxide generation, we conclude that even though superoxide is
11 generated in both AVA-MAPbI₃ and MAPbI₃ films, AVA located at grain boundaries is able to
12 passivate surface defect sites, resulting in enhanced resistivity to oxygen induced degradation.
13 These results are discussed in terms of their implications for the design of environmentally
14 stable perovskite solar cells.

15

16 **Main text**

17 State of the art power conversion efficiencies (PCE) of laboratory scale organohalide lead
18 perovskite solar cells (PSC) are now exceeding 22%, approaching PCEs achieved with silicon
19 photovoltaics.^{1,2} Interest in these solar cells is further motivated by their band gap tunability,
20 high trap state tolerance, high absorption coefficients and potentially low fabrication costs.³⁻
21 ⁶ However, attaining long term PSC device stability is still one of the key challenges for
22 commercialization. This is particularly the case for devices exposed to environmental stress,
23 with moisture, temperature, oxygen, light, and combinations of these, all being identified as
24 potential causes of degradation.⁷⁻⁹ Among these environmental stresses, the combination of
25 oxygen and light has been shown to be a key degradation pathway for devices tested in
26 ambient air under 1 Sun illumination.⁷ This degradation pathway has been shown to be
27 associated with the light driven reduction of oxygen to superoxide (O₂⁻).¹⁰ Several approaches,
28 including for example introducing a superoxide scavenger, and tuning perovskite composition
29 via cation/halide substitution, have been shown to be promising routes to enhance the
30 stability of organohalide lead perovskite materials and devices under light and oxygen
31 environmental stress.¹¹⁻¹³

32

33 Among the range of thin film PSC architectures reported in the literature to date, the screen
34 printed HTM free ('triple mesoscopic stack') architecture with carbon top electrode (c-PSC) is
35 attracting particular interest due to its potentially low production costs, scalability and
36 promising stability.¹⁴ These devices comprise two layers of mesoporous inorganic metal oxide
37 (TiO₂ and ZrO₂) and carbon top electrode, all infiltrated with perovskite light absorber
38 methylammonium lead iodide (MAPbI₃) employing aminovaleric acid (AVA) iodide as a
39 processing additive.¹⁴ The fully printable device processing makes this architecture
40 particularly attractive for scaling to large area fabrication.^{15,16} Unencapsulated devices
41 showed remarkable stability, exhibiting stable performance over 1000 hour under full sun
42 illumination without encapsulation,¹⁴ and over 1 year stability for encapsulated devices.¹⁷
43 Although enhanced stability against moisture has been suggested to be related to either the
44 ability of the zwitterionic AVA ligand to crosslink between the perovskite crystallites or to the
45 tendency of AVA to drive the formation of 2D perovskite layers,¹⁷⁻¹⁹ the origin of this
46 promising stability and particularly the device's increased resistance to light and oxygen
47 induced degradation, has not been determined to date.

1 In the study herein, we focus on the origin of the enhanced operational stability of
2 unencapsulated c-PSC devices observed with the addition of AVA to the MAPbI₃ film (AVA-
3 MAPbI₃). Unencapsulated c-PSC devices with AVA-MAPbI₃ are shown to exhibit ~ 40 times
4 longer lifetimes than devices with MAPbI₃ under full sun illumination in ambient air.
5 Remarkably, we find an analogous stability enhancement under similar stress conditions for
6 planar thin films of neat AVA-MAPbI₃ versus MAPbI₃ deposited directly onto glass substrates,
7 indicating this enhancement is not related to the MAPbI₃ / TiO₂ interface. Employing low-
8 energy ion scattering spectroscopy and time-dependent photoluminescence, we conclude
9 that, even though superoxide is generated in both AVA-MAPbI₃ and MAPbI₃ films, AVA
10 located at grain surfaces is able to passivate defect sites, resulting in enhanced resistivity to
11 oxygen induced degradation.

12
13 Multilayer screen printed mesoscopic stacks, comprising FTO/compact TiO₂/mesoporous
14 TiO₂/mesoporous ZrO₂/mesoporous carbon, were fabricated using thermal annealing method
15 as reported previously (Figure 1a).¹⁴ These stacks were then infiltrated with MAPbI₃, or
16 MAPbI₃ with 3% molar ratio of aminovaleric acid (AVA, Figure 1b), to complete the c-PSC
17 devices. Initial power conversion efficiencies for MAPbI₃ devices averaged 10.8% (champion
18 11.1%) and AVA-MAPbI₃ devices averaged 8.7% (champion 9.1%), which are reasonable for
19 fully printed devices (Figure S1a).^{14,20} These device PCEs are mask-area dependent as we
20 reported previously (Figure S1b and S1c) because of the poor conductivity of the carbon
21 electrode limiting the fill factor.²¹ MAPbI₃ and AVA-MAPbI₃ c-PSC devices were aged in
22 ambient air (RH ~15%) under 1 sun illumination provided by LEDs without encapsulation. The
23 devices were kept at open circuit voltage (Voc), and current-voltage scans undertaken every
24 30 minutes. As indicated in Figure 1c, the MAPbI₃ device rapidly lost 50% PCE within 2 hours,
25 while the AVA-MAPbI₃ device required more than 86 hours for an equivalent efficiency loss.
26 We note that aging devices at Voc can result in a more severe device degradation than at
27 maximum power point or short circuit.²² We previously reported that c-PSC with MAPbI₃
28 active layer showed outstanding ambient air (RH ~50%) shelf-lifetime (>3000 hours),²¹
29 indicating that dark humidity exposure does not limit the lifetime of c-PSC studied herein.
30 Therefore, as reported previously for analogous degradation studies of conventional
31 architecture PSC (FTO/compact-TiO₂/mesoporous-TiO₂/MAPbI₃/spiro-OMeTAD/Au), the
32 device degradation observed in Figure 1c can be assigned to light and oxygen stress, with the
33 AVA additive resulting in a 40-fold increase in device lifetime under 1 Sun illumination in
34 ambient air.

35
36 In order to address the origin of this enhanced stability with AVA, we first investigated
37 whether the enhanced stability in the presence of AVA is associated with the MAPbI₃ / TiO₂
38 interface. It has previously been suggested that the AVA, which contains both amine group
39 and carboxyl acid groups, can function as a crosslinking agent between mesoporous TiO₂ and
40 MAPbI₃.²³ To address this possibility, compact MAPbI₃ and AVA-MAPbI₃ thin films were
41 directly deposited on glass slides without any mesoporous TiO₂ layer and then aged with the
42 same air / light environmental stress as employed for the c-PSC devices in Figure 1c. Film
43 degradation was tracked optically by detecting the RGB photobleaching of the perovskite
44 films with a CCD camera (See ESI for details).¹³ We expected that if the enhancement was due
45 to the crosslinking effect of AVA, both AVA-MAPbI₃ and MAPbI₃ films should display similar
46 stability in the absence of mesoporous TiO₂. However, as shown in Figure 2a, the MAPbI₃ thin
47 film showed 50% photobleaching in 8 hours, while the AVA-MAPbI₃ took more than 108 hours

1 to display a similar equal level of photobleaching. This enhancement of thin film stability in
2 the absence of TiO_2 , which is of similar magnitude to the increase in device stability, clearly
3 indicates that AVA increases the stability of MAPbI_3 independently of any cross-linking effects
4 with TiO_2 .

5
6 We turn now to elucidating the origin of the enhanced stability of AVA- MAPbI_3 thin films
7 relative to MAPbI_3 under light and oxygen stress. SEM images of the MAPbI_3 and AVA- MAPbI_3
8 thin films are shown in Figure 2b and 2c. It is apparent that the MAPbI_3 film has larger grain
9 sizes than the AVA- MAPbI_3 film. It has previously been reported that perovskite
10 decomposition initiates at grain boundaries and surfaces, typically with smaller grain sizes
11 accelerating device degradation.^{9,24} In contrary, improved stability in AVA- MAPbI_3 is
12 observed despite its smaller grain size. Thus, it can be concluded that this enhancement in
13 stability does not originate from grain size differences.

14
15 As oxygen/light induced degradation has been shown to be initiated from perovskite grain
16 boundaries and surface,⁹ we suggest AVA is located at the termination of perovskite lattice.
17 Herein, low-energy ion scattering (LEIS) spectroscopy was used to detect the surface first
18 atomic layer of the film (Figure 3a). Firstly, the energy range between 0-1600 eV tells us about
19 the presence of H on the surface; the higher decaying signal indicates that AVA- MAPbI_3 thin
20 film has a higher concentration of H atoms on its surface. Secondly, since the yield has been
21 dose corrected and the measurement was conducted below the static limit, the normalised
22 data indicate lower concentrations of Pb and I atoms detected for AVA- MAPbI_3 compared to
23 MAPbI_3 . This is indicative of the presence of AVA molecules on AVA- MAPbI_3 film surface, as
24 illustrated in Figure 3b. As herein the AVA cations are directly mixed into the MAPbI_3 precursor
25 solution, rather than deposited as additional AVA cation layer on a preformed MAPbI_3 film, it
26 appears very likely that AVA molecules will also be present at grain boundaries, terminating
27 MAPbI_3 crystallites. Such terminations on crystallites may function as physical barriers to
28 protect MAPbI_3 from oxygen induced degradation.

29
30 Sun et al. have previously observed that perovskite films with higher defect densities are
31 degraded faster under oxygen and light stress.⁹ Oxygen/light degradation has also been
32 suggested to be postponed by passivating surface defects using iodide salts or fullerene
33 derivatives.^{11,24} As such, we now turn to considering whether the enhanced stability of AVA-
34 MAPbI_3 films observed herein may be associated with passivation of surface defects by AVA.
35 Photoluminescence (PL) has been shown to be a sensitive probe of defect densities in MAPbI_3
36 films.²⁵ In Figure 3c, UV-Vis of these films did not show an obvious shift, indicating AVA-
37 MAPbI_3 films have the same absorption and optical band gap as MAPbI_3 films. However, these
38 films do show significant differences in steady-state photoluminescence (Figure 3d). Firstly,
39 the AVA- MAPbI_3 films exhibit three times higher PL intensity than the MAPbI_3 films, indicating
40 AVA passivates defect states in the perovskite which would lead to non-radiative
41 recombination. Secondly, the PL peak position is shifted from 770 nm (MAPbI_3) to 763 nm
42 (AVA- MAPbI_3). It has been previously reported that the MAPbI_3 PL peak can blue shift when
43 trap/defect states are passivated.²⁶ Therefore, we can conclude that AVA is able to passivate
44 trap / defect states in MAPbI_3 films, consistent with previous studies correlating lower defect
45 densities and enhanced stability against oxygen/light induced degradation.⁹

1 We note that despite this trap state passivation, AVA-MAPbI₃ devices exhibited slightly lower
2 device efficiencies. This most likely results from differences in the procedure for perovskite
3 deposition (one-step rather than two-step, see ESI in details), which are likely to result in less
4 complete infiltration of the precursor solution and/or crystallinity of the resulting perovskite
5 light absorber.

6
7 In addition to the correlation between defect density and stability against light/oxygen
8 induced degradation reported herein and previously, it has also been reported that oxygen
9 can itself fill defects in MAPbI₃, resulting in increased PL emission.^{27,28} As such, the impact of
10 oxygen on film photoluminescence can have several different effects: it can act as an acceptor
11 for MAPbI₃ electrons, resulting in a reduction in PL intensity; it can insert into surface MAPbI₃
12 defects, reducing the effect of electron trapping and thus increasing PL intensity; finally it can,
13 in the presence of light, result in photodegradation of MAPbI₃, decreasing PL intensity. In
14 order to unravel these complex interactions between oxygen and MAPbI₃ and their impact
15 upon PL intensity, we monitored the PL of MAPbI₃ and AVA-MAPbI₃ films as a function of time
16 after oxygen exposure (Figures 4a-c). Samples were initially stored in N₂ filled quartz cuvettes,
17 and 20 vol% oxygen introduced into the cuvette after the first PL scan. We observed that the
18 PL intensity of MAPbI₃ films increased over time following oxygen exposure (Figure 4a),
19 consistent with previous reports.^{27,28} This increase is attributed, as previously, to oxygen
20 binding to surface defects, partially passivating these defects and reducing their tendency to
21 function as electron traps (Pathway 1 in the insert to Figure 4c). This increase in PL intensity
22 saturated after 1000 seconds, after this it started to decrease, alongside the appearance of a
23 low energy tail of the PL spectrum (Figure S2). Such a low energy tail of the PL is also observed
24 in MAPbI₃ film with excess PbI₂ or MAI in the literature, and is indicative of superoxide induced
25 degradation of MAPbI₃.^{29,30} As such, this decrease at long times is assigned to MAPbI₃
26 degradation, with the timescale being consistent with the photobleaching data shown in
27 Figure 2 above. In contrast, AVA-MAPbI₃ films showed a pronounced decrease of PL intensity
28 when exposed to oxygen in Figure 4b (although from a much higher initial value). The
29 timescale for this decrease in PL intensity (decays half-time of ~150 s) is similar to timescales
30 previously reported for oxygen to diffuse into MAPbI₃ grain boundaries.²⁴ This PL quenching
31 cannot attributed to perovskite degradation as AVA-MAPbI₃ has shown to be stable on this
32 time scale in Figure 2a. Rather this quenching of PL in the presence of oxygen can be
33 attributed to electron transfer from AVA-MAPbI₃ grains to oxygen molecules in grain
34 boundaries (pathway 2 in Figure 4c), resulting in superoxide formation. This observation is
35 consistent with surface defect states already being occupied by AVA in this film, such that
36 oxygen binding into such states is inhibited.

37
38 To sum up, we suggest there are two pathways leading to the PL intensity changes on the
39 100-1000s timescale in the films studied herein. This timescale corresponds to the timescale
40 of oxygen diffusion into film grain boundaries, but it is faster than the timescale of light and
41 oxygen induced photodegradation. Oxygen binding into perovskite surface defects can result
42 in PL intensity increasing (Pathway 1 in Figure 4c), while oxygen in grain boundaries which
43 does not incorporate into perovskite defects can reduce PL intensity (Pathway 2 in Figure 4c).
44 Because the MAPbI₃ film is rich in unpassivated surface defects, Pathway 1 dominates over
45 Pathway 2, leading to the enhanced PL intensity. However such oxygen binding into surface
46 defects does not protect the film against light and oxygen induced degradation, consistent
47 with the reduction in PL intensity observed at long times, correlated with the photobleaching

1 data in Figure 2. In contrast, as AVA has already effectively passivated these defects in AVA-
2 MAPbI₃, oxygen is unable to incorporate into these defects and pathway 1 is inactive.
3 Therefore, the Pathway 2 dominates in AVA-MAPbI₃ films, resulting in the observed reduction
4 in PL intensity. These counterpoised effects of oxygen on the PL intensity of MAPbI₃ and AVA-
5 MAPbI₃ films clearly illustrate the differing effects of oxygen on the film photophysics, as
6 discussed further below.

7
8 Previously, we have proposed that the oxygen/light degradation is mediated by superoxide,
9 which is generated when the oxygen accepts a photoexcited electron from MAPbI₃.²⁴ To
10 evaluate the formation of superoxide (O₂⁻) in MAPbI₃ and AVA-MAPbI₃ films, we monitored
11 the superoxide formation by the hydroethidine (HE) molecular fluorescent probe, which
12 exhibits a characteristic increase in fluorescence following O₂⁻ exposure, as previously
13 reported.¹⁰ As plotted in Figure 4d, it is apparent that an AVA-MAPbI₃ film shows higher
14 generation of free superoxide than a MAPbI₃ film. As AVA-MAPbI₃ demonstrates superior thin
15 film stability to MAPbI₃, we can conclude that this enhanced stability derives not from
16 suppression of superoxide generation but rather from higher resistance to superoxide
17 induced degradation. We note that we have previously reported an analogous result in a
18 comparison of the stability of MAPbI₃ and MAPbBr₃ films, where we observed efficiently
19 generated superoxide but resistance to superoxide mediated degradation, attributed in this
20 case to the superior chemical stability of MAPbBr₃.¹³ Our observation that AVA-MAPbI₃ films
21 generate more superoxide than MAPbI₃ can most likely be attributed to their higher density
22 of grain boundaries (due to their small grain sizes), facilitating oxygen diffusion in, and
23 superoxide diffusion out, of these films.

24
25 Based upon these results and previous literature, we summarise by proposing a simple model
26 to explain the enhanced stability of AVA-MAPbI₃ to light and oxygen induced degradation, as
27 illustrated in Figure 5. In the absence of AVA, oxygen can bind to surface defect sites on
28 MAPbI₃ crystallites (Process 'A' in Figure 5). This results in a modest enhancement of PL
29 intensity due to partial surface defect state passivation. AVA can also bind to such surface
30 defects, resulting in a much more effective defect site passivation, and preventing subsequent
31 oxygen binding to these sites. Photoexcitation of both MAPbI₃ and AVA-MAPbI₃ in the
32 presence of oxygen can result in the reduction of oxygen in grain boundaries, resulting in free
33 superoxide generation, as observed in our superoxide probe measurements (Figure 4d).
34 However, as suggested previously, degradation of perovskite by superoxide requires access
35 to surface defects.²⁴ The passivation of surface defects by AVA prevents superoxide mediated
36 degradation and greatly enhances stability. In the absence of AVA, superoxide is able to access
37 surface defects and induce degradation (Process 'B' in Figure 5). It is also possible this
38 degradation may result from the reduction of oxygen already bound in defect sites (Process
39 'A'), although our data cannot separately observe this. Overall these results indicate that the
40 enhanced stability of AVA-MAPbI₃ films results from the passivation of surface defect sites
41 which otherwise can mediate superoxide induced degradation.

42
43 In conclusion, we demonstrate that using AVA-MAPbI₃ as an active layer in c-PSC structure
44 device results in ~40 times longer operational lifetime than MAPbI₃ in ambient air (RH ~15%).
45 This improvement is also observed in thin film stability, revealing it is correlated to perovskite
46 itself rather than the interaction between perovskite and any other interlayers. Consequently,
47 it may be possible to apply this passivation technique to stabilise other device architectures.

1 AVA is found to be located at the grain surface of MAPbI₃, passivating surface defects. The
2 AVA-MAPbI₃ with lower defects density demonstrate higher resistance to oxygen and light
3 stress than MAPbI₃. Even though AVA-MAPbI₃ film generates more superoxide than MAPbI₃
4 film, AVA-MAPbI₃ demonstrates higher superoxide resistivity. The passivation of surface
5 defects by AVA results in physical barrier to protect MAPbI₃ from superoxide induced
6 degradation in grain boundary, prolonging the lifetime of both thin films and devices under
7 oxygen/light stress. Therefore, in this study we deduce the origin of improved stability of AVA-
8 MAPbI₃ c-PSC device and highlight the strategy of passivation of perovskite's grain
9 termination to enhance its resistance to oxygen/light degradation.

10 **Conflicts of interest**

11 There are no conflicts to declare.

12 **Acknowledgment**

13 We thank Welsh government funded Sêr Solar project, as well as the EPSRC Plastic
14 Electronics CDT, the UKRI Global Challenge Research Fund project SUNRISE (EP/P032591/1),
15 Self - assembly Perovskite Absorber layers - Cells Engineered into Modules Project
16 (EP/M01524/2), SPECIFIC IKC (EP/N02083/1) and the CSC for financial support, as well as
17 Xiaoe Li for technical support.

18

Reference

- 1 W. S. Yang, B.-W. Park, E. H. Jung, N. J. Jeon, Y. C. Kim, D. U. Lee, S. S. Shin, J. Seo, E. K. Kim, J. H. Noh and S. Il Seok, *Science (80-.)*, 2017, **356**, 1376–1379.
- 2 K. Yoshikawa, H. Kawasaki, W. Yoshida, T. Irie, K. Konishi, K. Nakano, T. Uto, D. Adachi, M. Kanematsu, H. Uzu and K. Yamamoto, *Nat. Energy*, 2017, **2**, 17032.
- 3 J. H. Noh, S. H. Im, J. H. Heo, T. N. Mandal and S. Il Seok, *Nano Lett.*, 2013, **13**, 1764–1769.
- 4 Z. Song, C. L. McElvany, A. B. Phillips, I. Celik, P. W. Krantz, S. C. Watthage, G. K. Liyanage, D. Apul and M. J. Heben, *Energy Environ. Sci.*, 2017, **10**, 1297–1305.
- 5 J.-H. Im, C.-R. Lee, J.-W. Lee, S.-W. Park and N.-G. Park, *Nanoscale*, 2011, **3**, 4088.
- 6 R. E. Brandt, V. Stevanović, D. S. Ginley and T. Buonassisi, *MRS Commun.*, 2015, **5**, 265–275.
- 7 D. Bryant, N. Aristidou, S. Pont, I. Sanchez-Molina, T. Chotchunangatchaval, S. Wheeler, J. R. Durrant and S. A. Haque, *Energy Environ. Sci.*, 2016, **9**, 1655–1660.
- 8 A. M. A. Leguy, Y. Hu, M. Campoy-Quiles, M. I. Alonso, O. J. Weber, P. Azarhoosh, M. Van Schilfhaarde, M. T. Weller, T. Bein, J. Nelson, P. Docampo and P. R. F. Barnes, *Chem. Mater.*, 2015, **27**, 3397–3407.
- 9 Q. Sun, P. Fassel, D. Becker-Koch, A. Bausch, B. Rivkin, S. Bai, P. E. Hopkinson, H. J. Snath and Y. Vaynzof, *Adv. Energy Mater.*, 2017, **1700977**, 20.
- 10 N. Aristidou, I. Sanchez-Molina, T. Chotchuangchutthaval, M. Brown, L. Martinez, T. Rath and S. A. Haque, *Angew. Chem. Int. Ed. Engl.*, 2015, **54**, 1–6.
- 11 C.-T. Lin, S. Pont, J. Kim, T. Du, S. Xu, X. Li, D. Bryant, M. A. Mclachlan and J. R. Durrant, *Sustain. Energy Fuels*, 2018, **2**, 1686–1692.
- 12 M. Saliba, T. Matsui, J.-Y. Seo, K. Domanski, J.-P. Correa-Baena, M. K. Nazeeruddin, S. M. Zakeeruddin, W. Tress, A. Abate, A. Hagfeldt and M. Grätzel, *Energy Environ. Sci.*, 2016, **9**, 1989–1997.
- 13 S. Pont, D. Bryant, C.-T. Lin, N. Aristidou, S. Wheeler, X. Ma, R. Godin, S. A. Haque and J. R. Durrant, *J. Mater. Chem. A*, 2017, **5**, 9553–9560.
- 14 A. Mei, X. Li, L. Liu, Z. Ku, T. Liu, Y. Rong, M. Xu, M. Hu, J. Chen, Y. Yang, M. Grätzel and H. Han, *Science (80-.)*, 2014, **345**, 295–298.
- 15 M. Hu, L. Liu, A. Mei, Y. Yang, T. Liu and H. Han, *J. Mater. Chem. A Mater. energy Sustain.*, 2014, **2**, 17115–17121.
- 16 Y. Hu, S. Si, A. Mei, Y. Rong, H. Liu, X. Li and H. Han, *Sol. RRL*, 2017, **1**, 1600019.
- 17 G. Grancini, C. Roldán-Carmona, I. Zimmermann, E. Mosconi, X. Lee, D. Martineau, S. Narbey, F. Oswald, F. DeAngelis, M. Graetzel and M. K. Nazeeruddin, *Nat. Commun.*, 2017, **8**, 15684.
- 18 H. Tsai, W. Nie, J.-C. Blancon, C. C. Stoumpos, R. Asadpour, B. Harutyunyan, A. J. Neukirch, R. Verduzco, J. J. Crochet, S. Tretiak, L. Pedesseau, J. Even, M. A. Alam, G. Gupta, J. Lou, P. M. Ajayan, M. J. Bedzyk, M. G. Kanatzidis and A. D. Mohite, *Nature*, 2016, **536**, 312–316.
- 19 X. Li, M. Ibrahim Dar, C. Yi, J. Luo, M. Tschumi, S. M. Zakeeruddin, M. K. Nazeeruddin, H. Han and M. Grätzel, *Nat. Chem.*, 2015, **7**, 703–711.
- 20 C. Chan, Y. Wang, G. Wu and E. W. Diau, *J. Mater. Chem. A Mater. energy Sustain.*, 2016, **4**, 3872–3878.
- 21 J. Baker, K. Hooper, S. Meroni, A. Pockett, J. McGettrick, Z. Wei, R. Escalante, G. Oskam, M. Carnie and T. Watson, *J. Mater. Chem. A*, 2017, **5**, 18643–18650.
- 22 K. Domanski, E. A. Alharbi, A. Hagfeldt, M. Grätzel and W. Tress, *Nat. Energy*, 2018, **3**, 61–67.

- 23 Y. C. Shih, Y. B. Lan, C. S. Li, H. C. Hsieh, L. Wang, C. I. Wu and K. F. Lin, *Small*, 2017, **13**, 1–10.
- 24 N. Aristidou, C. Eames, I. Sanchez-Molina, X. Bu, J. Kosco, M. S. Islam and S. A. Haque, *Nat. Commun.*, 2017, **8**, 15218.
- 25 N. K. Noel, A. Abate, S. D. Stranks, E. S. Parrott, V. M. Burlakov, A. Goriely and H. J. Snaith, *ACS Nano*, 2014, **8**, 9815–9821.
- 26 Y. Shao, Z. Xiao, C. Bi, Y. Yuan and J. Huang, *Nat. Commun.*, 2014, **5**, 1–7.
- 27 R. Brenes, D. Guo, A. Osherov, N. K. Noel, C. Eames, E. M. Hutter, S. K. Pathak, F. Niroui, R. H. Friend, M. S. Islam, H. J. Snaith, V. Bulović, T. J. Savenije and S. D. Stranks, *Joule*, 2017, **1**, 155–167.
- 28 Y. Tian, M. Peter, E. Unger, M. Abdellah, K. Zheng, T. Pullerits, A. Yartsev, V. Sundström and I. G. Scheblykin, *Phys. Chem. Chem. Phys.*, 2015, **17**, 24978–24987.
- 29 T. Du, J. Kim, J. Ngiam, S. Xu, P. R. F. Barnes, J. R. Durrant and M. A. McLachlan, *Adv. Funct. Mater.*, 2018, 1801808.
- 30 V. Kapoor, A. Bashir, L. J. Haur, A. Bruno, S. Shukla, A. Priyadarshi, N. Mathews and S. Mhaisalkar, *Energy Technol.*, 2017, **5**, 1880–1886.

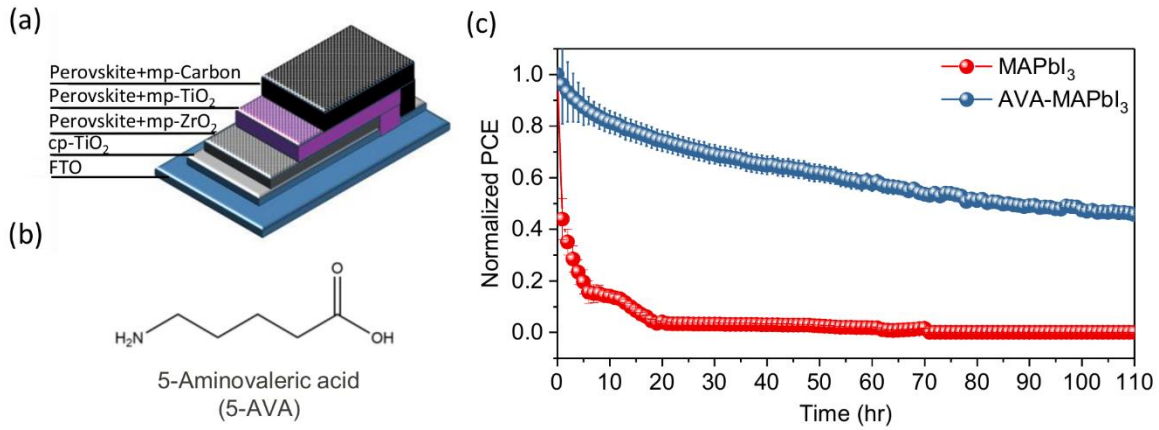


Figure 1. (a) Device configuration of multi-layer screen printed mesoporous stack perovskite solar cell (c-PSC) consisted of FTO/compact-TiO₂/mesoporous-TiO₂/mesoporous-ZrO₂/mesoporous-carbon. (b) Chemical structure of 5-aminovaleric acid. (c) Normalized device stability of MAPbI₃ and AVA-MAPbI₃ devices. Stability were measured under ambient air (RH ~15%) and continuous illumination provided by LED. Light intensity of LED was calibrated to provide equivalent J_{sc} measured under AM 1.5 solar simulator with 1 sun intensity.

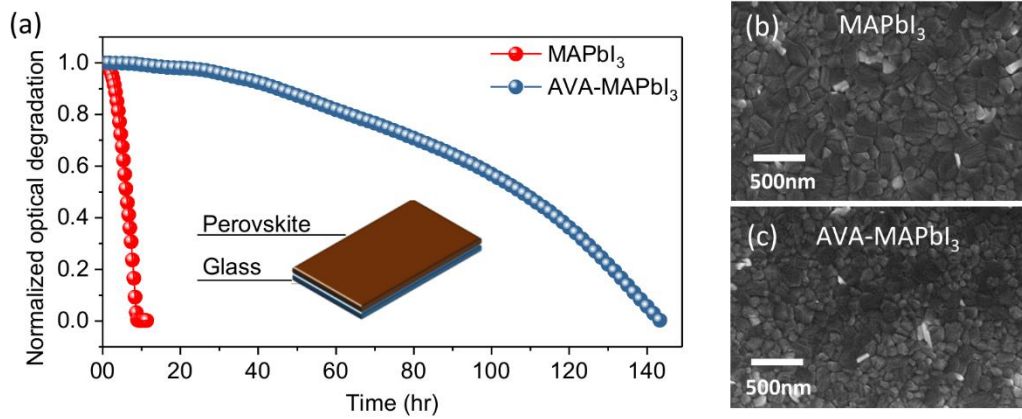


Figure 2. (a) Normalized optical degradation of MAPbI₃ and AVA-MAPbI₃ thin film on glass in ambient air (RH ~15%) with full sun illumination provided by LED array. SEM images of (b) MAPbI₃ and (c) AVA-MAPbI₃.

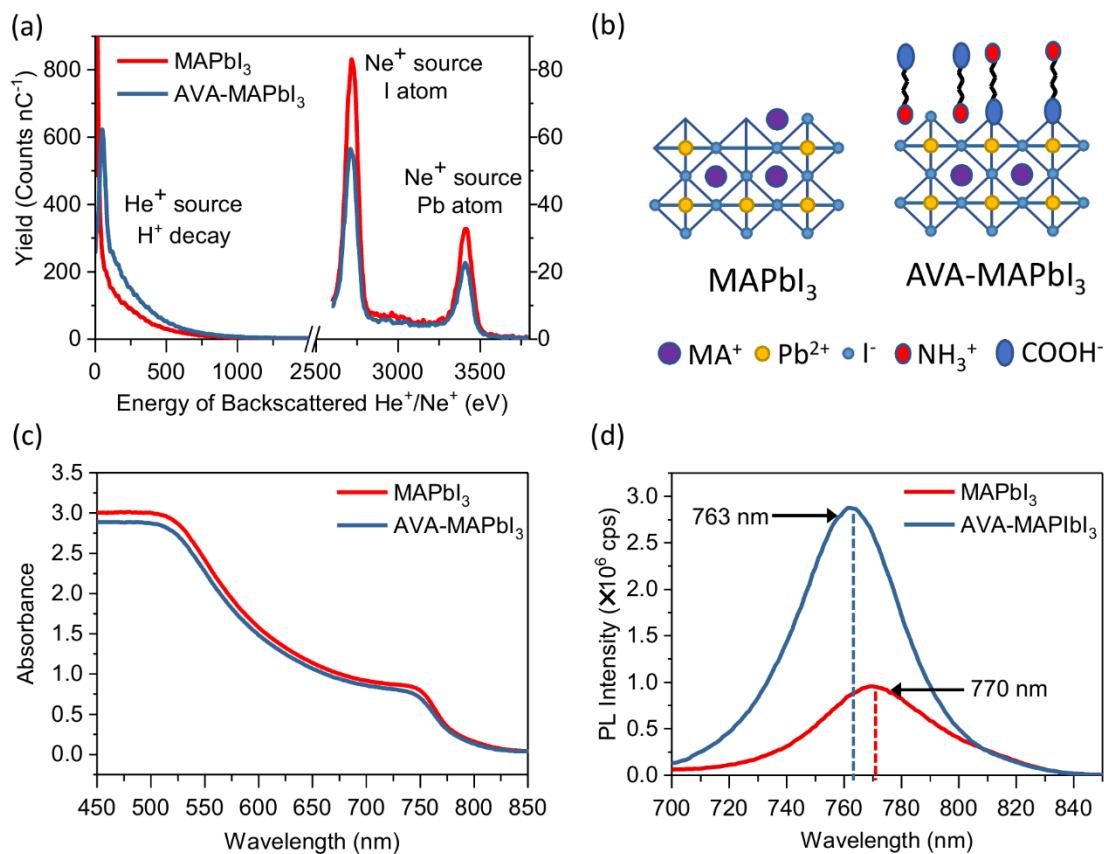


Figure 3. (a) Low-energy ion scattering (LEIS) measurement of MAPbI₃ and AVA-MAPbI₃ films. Ne⁺ plasma was used to detect Pb and I atoms. He⁺ plasma was used to detect H⁺ decay. (b) Schematic representation of AVA passivation at lattice termination of MAPbI₃ (c) UV-visible and (d) steady-state photoluminescence (PL) spectra of MAPbI₃ and AVA-MAPbI₃ films. PL spectra were measured under full sun illumination provided by LED array with 700 nm low pass filter.

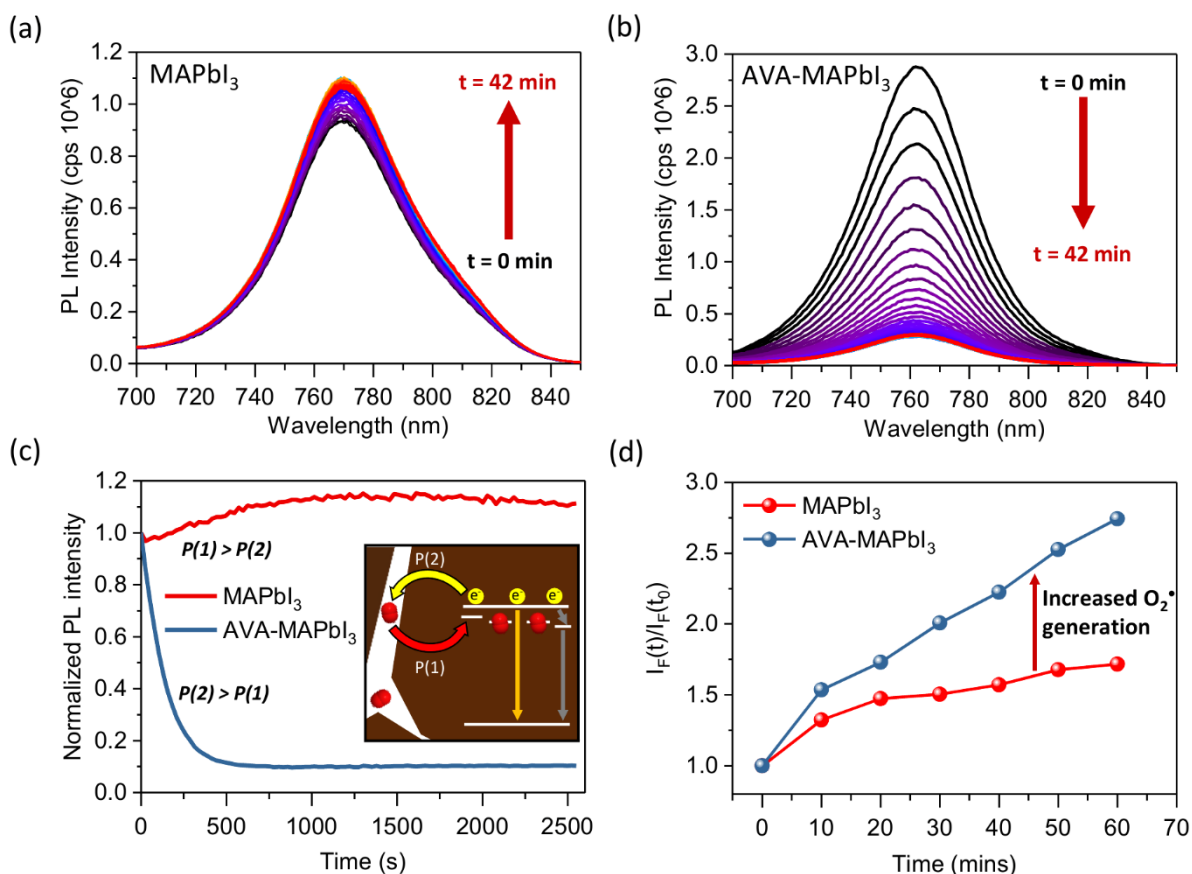


Figure 4. PL spectra of (a) MAPbI₃ and (b) AVA-MAPbI₃ as a function of time after exposure to oxygen (employing LED excitation as for Figure 3). (c) PL peak intensity versus time following exposure to oxygen, taken from the data in (a) and (b). Inserted illustration diagram provides two possible pathway of PL changes. Pathway1 is the oxygen incorporated into perovskite defects leading to increased PL intensity. Pathway2 is the oxygen at grain boundaries quenching the PL intensity. (d) Fluorescence intensity of a molecular probe for superoxide as a function of perovskite film irradiation time in the presence of oxygen. Fluorescence intensity probed at 610 nm with excitation at 520 nm, where $I_F(t)$ is the fluorescence intensity at time t , and $I_F(t_0)$ is at 0 minutes. The $I_F(t)/I_F(t_0)$ ratio is measure of the amount of superoxide generated by irradiation of the perovskite films.

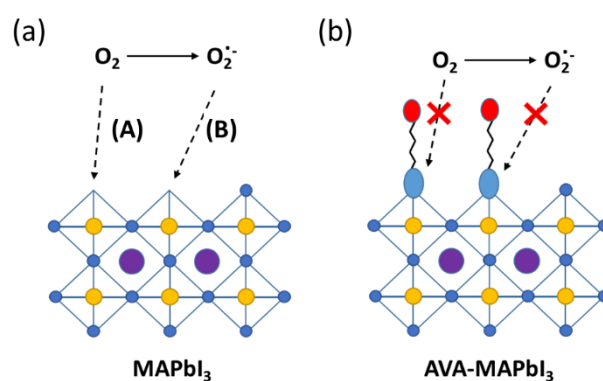


Figure 5. Schematic representation of enhanced stability resulting from AVA passivation of surface defect sites of MAPbI₃. In the absence of AVA (a), oxygen can access iodide vacancies at grain boundaries, resulting under irradiation in superoxide mediated photodegradation. In the presence of AVA (b), AVA binds to these iodide vacancies, inhibiting this degradation.